EuroIntervention 2023;18:e1120-e1128 published online ahead of print October 2022 ■ published online e-edition February 2023

Translational value of preclinical models for renal denervation: a histological comparison of human versus porcine renal nerve anatomy

Yu Sato[1], MD; Andrew S.P. Sharp[2], MD; Felix Mahfoud[3], MD; Stefan Tunev[4], DVM; Ashley Forster[1], BS; Matthew Ellis[1], BS; Ana Gomez[1]; Roma Dhingra[1]; Jeremy Ullman[1]; Markus Schlaich[5], MD; David Lee[6], MD; Julie Trudel[4], PhD; Douglas A. Hettrick[4], PhD; David E. Kandzari[7], MD; Renu Virmani[1], MD; Aloke V. Finn[1,8]*, MD

1. CVPath Institute Inc., Gaithersburg, MD, USA; 2. University Hospital of Wales, Cardiff, UK; 3. Department of Internal Medicine III, Cardiology, Angiology and Intensive Care Medicine, Saarland University Hospital, Hamburg, Germany; 4. Medtronic, Santa Rosa, CA, USA; 5. University of Western Australia, Perth, Australia; 6. Stanford Hospital and Clinics, Palo Alto, CA, USA; 7. Department of Cardiovascular Surgery, Marcus Valve Center, Piedmont Heart Institute, Atlanta, GA, USA; 8. University of Maryland, Baltimore, MD, USA

This paper also includes supplementary data published online at: https://eurointervention.pcronline.com/doi/10.4244/EIJ-D-22-00369

KEYWORDS

- hypertension
- renal sympathetic denervation
- resistant hypertension

Abstract

Background: Preclinical models have provided key insights into the response of local tissues to radiofrequency (RF) renal denervation (RDN) that is unobtainable from human studies. However, the anatomic translatability of these models to the procedure in humans is incompletely understood.

Aims: We aimed to compare the renal arterial anatomy in normotensive pigs treated with RF-RDN to that of human cadavers to evaluate the suitability of normotensive pigs for determining the safety of RF-RDN.

Methods: Histopathologic analyses were performed on RF-treated renal arteries in a porcine model and untreated control renal arteries. Similar analyses were performed on untreated renal arteries from human cadavers.

Results: In both human and porcine renal arteries, the median number of nerves was lower in the more distal sections (the numbers in the proximal, middle, distal, 1st bifurcation, and 2nd bifurcation sections were 65, 58, 47, 22.5, and 14.7 in humans, respectively, and 39, 26, 29, 16.5, and 9.3 in the porcine models, respectively). Renal nerves were common in the regions between arteries and adjacent veins, but only 3% and 13% of the renal nerves in humans and pigs, respectively, were located behind the renal vein. The semiquantitative score of RF-induced renal arterial nerve necrosis was significantly greater at 7 days than 28 days (0.98 vs 0.75; p=0.01), and injury to surrounding organs was rarely observed.

Conclusions: The distribution of nerve tissue and the relative distribution of extravascular anatomic structures along the renal artery was similar between humans and pigs, which validates the translational value of the normotensive porcine model for RDN.

**Corresponding author: CVPath Institute Inc., 19 Firstfield Road, Gaithersburg, MD 20878, USA.*
E-mail: afinn@cvpath.org

SUBMITTED ON 18/04/2022 - REVISION RECEIVED ON 23/07/2022 - ACCEPTED ON 11/08/2022

DOI: 10.4244/EIJ-D-22-00369

Abbreviations

IQR interquartile range
RDN renal denervation
RF radiofrequency
SD standard deviation
SE standard error

Introduction

Over 30% of adults worldwide have hypertension, yet blood pressure is adequately controlled in only a fraction of the global hypertensive population[1]. Poor control rates among people with hypertension, ranging from 5-50% in 2019, contribute to global cardiovascular risk and persist despite the availability of safe and effective lifestyle interventions and drug therapies[2]. Percutaneous renal denervation (RDN) using various energy sources, including radiofrequency (RF), ultrasound energy or injection of alcohol, has shown the potential to complement hypertension management by interrupting the nerve signalling between the kidney and the brain. Indeed, several recent randomised, sham-controlled trials using different techniques have reported statistically and clinically significant blood pressure reductions in various populations with uncontrolled hypertension in both the presence and absence of concomitant drug therapy[3,4,5,6]. However, the microscopic physiology of renal nerve destruction post-RDN is difficult to study in human subjects and most of the scientific basis for renal nerve ablation has therefore been determined from animal models[7,8,9]. The normotensive porcine model is the most widely applied to investigate the safety of RDN procedures, but its translational value to humans remains incompletely understood. We compared similar histological studies in untreated human cadavers and normotensive pigs treated with RF-RDN to evaluate the clinical utility of the porcine model.

Methods

PORCINE STUDIES: SAFETY ASSESSMENT OF RENAL ARTERIAL DENERVATION WITH RADIOFREQUENCY CATHETERS

Animal studies were performed in accordance with the Guide for the Care and Use of Laboratory Animals of the National Institutes of Health (Publication Number 85-23, revised 1996). The experimental methods have been previously described[8]. Briefly, Yorkshire domestic farm pigs of either sex, weighing between 35 and 50 kg, were studied according to an approved Institutional Animal Care and Use Committee protocol, in compliance with the Animal Welfare Act and the US Food and Drug Administration regulations and their amendments. Anaesthesia was induced, arterial access was achieved under sterile conditions, and a multielectrode RF-RDN catheter (Symplicity Spyral; Medtronic) was advanced under fluoroscopic guidance into the renal artery and positioned via a standard guide catheter and guidewire. Simultaneous RF ablations with 4 electrodes in a helical pattern were delivered in each renal artery and in suitable post-1st bifurcation branch segments. No ablations were performed beyond the first level of renal artery bifurcation. Following treatment, the catheter was removed, the vascular access site was sealed using standard techniques, and the animals were allowed to recover. Animals were euthanised via an overdose of pentobarbital after 7 (N=12 pigs) and 28 days (N=16 pigs), and tissue samples were immediately obtained to evaluate the impact of time on observable ablation tissue effects.

Using a semiquantitative scoring method, a histopathologic analysis was performed on the treated regions to evaluate the response of surrounding structures, including the ureter, kidneys, lymph nodes, skeletal muscles and adrenal glands, to RF energy. Both the type and magnitude of changes to the peri-arterial nerves were evaluated semiquantitatively, including damage incurred directly in the plane of the section lying directly in the path of treatment or along the vessel length, upstream or downstream. Degenerative nerve changes included vacuolisation, necrosis, and the formation of digestion chambers associated with injury. Necrotic changes ranged from pyknosis/karyorrhexis of individual neural nuclei to coagulative necrosis or frank coagulation of the nerve bundle. Similar criteria were applied to cellular level disorganisation of non-neural perivascular organs considering the impact on structure, architecture, and function. A score of 0 indicated no observable damage across the sample. For minimal or grade 1 injury, the nerve or collateral tissue was considered largely intact and likely to be functional but exhibiting subtle signs of damage. Moderate or grade 2 injury exhibited more notable changes that may have included inflammation, fibrosis, or swelling. Severe or grade 3 injury indicated overwhelming damage including marked necrosis, mineralisation, inflammation and/or fibrosis and, in the case of nerve tissue, endoneurium damage. Only moderate or severe injury (i.e., grade 2 or 3) were considered to be associated with thermal damage, since some cellular disruption (i.e., grade 1) can be observed in untreated samples[10].

UNTREATED HUMAN CADAVER AND HEALTHY PORCINE MODEL STUDIES: ANATOMICAL ASSESSMENT

The histopathologic assessment on healthy porcine renal arteries was performed to evaluate the anatomical relationship between human and porcine renal arteries and their surrounding structures. The processing of the porcine histologic slides was performed at Alizée Pathology (currently StageBio, Mt Jackson, VA, USA). Bilateral untreated renal arteries were collected from 8 Yorkshire domestic farm pigs of either sex, weighing between 35 and 50 kg. The protocol was approved by the Institutional Animal Care and Use Committee and was in compliance with the Animal Welfare Act and the US Food and Drug Administration regulations and their amendments.

The processing of histologic slides for human renal arteries was performed at the CVPath Institute (Gaithersburg, MD, USA). Bilateral human renal arteries with attached abdominal aorta and kidneys were collected from 10 autopsy subjects from our autopsy registry. The Institutional Review Board at the CVPath Institute approved this study. After a gross inspection, renal arteries were perfusion-fixed under physiological pressure (80 to 100 mmHg) with 10% neutral-buffered formalin via the abdominal aorta. Whole specimens were subsequently fixed in 10% neutral-buffered

formalin. Each renal artery from both porcine models and humans was subdivided into 5 segments from the ostium to the renal hilum (proximal, middle, distal, post-1st bifurcation, and post-2nd bifurcation). Each segment of the renal artery was further sectioned at 2-4 mm intervals and was submitted in a separate cassette for paraffin processing. Histologic sections were cut on a rotary microtome at 4-6 µm, mounted on charged slides, and stained with haematoxylin and eosin.

The histologic stained slides were magnified and digitised. Quantitative morphometry was performed using computerised planimetry software (ZEN 2; ZEISS). Measurements of the number of peri-arterial nerves and the presence or absence of peri-arterial structures, such as lymph nodes, neuroganglia, the kidneys, and the ureter, were taken. Nerves were considered "behind" the vein when a hypothetical line extending normally between the nerve and arterial wall passed through a renal vein.

STATISTICAL ANALYSIS

Results for continuous variables with normal distribution are shown as mean±standard error (SE) or deviation (SD). Results without normal distributions are shown as median and interquartile range (IQR). The Student's t-test was used to analyse the significance of differences for continuous results with normal distributions, whereas comparisons of results with non-parametric distributions were analysed using the Kruskal-Wallis test. Results were considered statistically significant if the probability (p) was <0.05. Analyses were performed using Prism software version 6 (GraphPad Software) or JMP software version 15.0 (SAS Institute).

Results

THE SPATIAL RELATIONSHIP BETWEEN THE RENAL ARTERY AND SURROUNDING ORGANS: A COMPARATIVE ANALYSIS OF THE HUMAN CADAVER AND THE PORCINE MODEL

The characteristics of the human autopsy subjects are shown in **Table 1**. The mean age was 46.7 years, 70% were male, and 50% of subjects had a history of hypertension. A total of 20 renal arteries from 10 human autopsy subjects were analysed, including 9,375 peri-arterial nerves from 179 histologic sections **(Table 2)**. For comparison with the human samples, 16 renal arteries from 8 healthy pigs were examined, including 5,902 peri-arterial nerves from 177 histologic sections **(Table 3)**. The mean diameter, length, and medial wall thickness of the main renal artery in the human

Table 1. Characteristics of human cases.

Case	N=10
Age, years	46.7±10.7
Sex (male)	7 (70)
Race (Caucasian/African American)	7 (70)/3 (30)
Body length, cm	175.3±7.8
Body weight, kg	89.4±14.0
BMI, kg/m^2	25.4±9.1
Obesity (BMI >30)	3 (30)
Hypertension	5 (50)
Sudden coronary death/non-coronary death	3 (30)/7 (70)

Values are shown as mean±standard deviation or number (%). BMI: body mass index

Table 2. Findings in human renal arteries among proximal, middle, distal, post 1st bifurcation, and post 2nd bifurcation.

	Proximal	Middle	Distal	Post-1st bifurcation	Post-2nd bifurcation	Total	*p*-value
Total no. of sections	36	31	24	49	39	179	
Total no. of nerves	2,465	2,042	1,310	1,992	1,564	9,373	
No. of nerves/section, median (IQR)	65 (50-88.8)	60 (43-83)	53 (32.5-73.8)	44 (23.5-52)	43 (20-55)	50 (31-66)	<0.0001
No. of renal artery/section, mean±SD	1.06±0.23	1.06±0.25	1.08±0.28	1.88±0.33	2.92±0.42		
No. of nerves/section corrected by no. of renal artery, median (IQR)	65 (50-88.8)	58 (39-83)	47 (31.7-73)	22.5 (12-26)	14.7 (8.5-18.7)	28 (58-16.3)	<0.0001
The number of sections with lymph nodes, n (%)	35 (97.2)	21 (67.7)	11 (45.8)	9 (18.4)	0 (0)	76 (42.5)	<0.0001
Distance between lymph node and renal artery, mm	2.6 (1.7-5.0)	2.9 (1.9-4.8)	2.5 (1.7-3.0)	NA	NA	2.6 (1.7-4.7)	0.77
The number of sections with neuroganglion, n (%)	35 (97.2)	26 (83.9)	17 (70.8)	13 (26.5)	4 (10.3)	95 (97.2)	<0.0001
Distance between neuroganglion and renal artery, mm	2.3 (1.4-4.6)	2.2 (1.3-5.1)	4.0 (2.5-7.3)	NA	NA	2.8 (1.5-5.9)	0.09
The number of sections with kidney, n (%)	0 (0)	0 (0)	3 (12.5)	12 (24.5)	23 (59.0)	38 (21.2)	<0.0001
Distance between kidney and renal artery, mm	0 (0-0)	0 (0-0)	5.9 (2.9-6.2)	NA	NA	5.9 (2.9-6.2)	NA
The number of sections with ureter, n (%)	0 (0)	0 (0)	1 (4.2)	8 (16.3)	14 (35.9)	23 (12.9)	<0.0001
Distance between ureter and renal artery, mm	0 (0-0)	0 (0-0)	6.8 (6.8-6.8)	NA	NA	6.8 (6.8-6.8)	NA
The number of sections with renal vein, n (%)	20 (55.6)	22 (71.0)	18 (75.0)	47 (95.9)	39 (100)	146 (81.6)	<0.0001
Distance between renal vein and renal artery, mm	3.8 (2.6-5.2)	2.8 (2.2-4.5)	2.3 (1.8-3.6)	NA	NA	2.9 (2.2-4.5)	0.0344
Total no. of nerves behind the renal vein, n	66	64	58	79	17	284	
Percentage of the number of nerves behind the renal vein expressed as a percentage of the total number of nerves	2.7	3.1	4.4	4.0	1.1	3.0	

IQR: interquartile range; SD: standard deviation

Table 3. Findings in porcine renal arteries among proximal, middle, distal, post-1st bifurcation, and post-2nd bifurcation.

	Proximal	Middle	Distal	Post-1st bifurcation	Post-2nd bifurcation	Total	*p*-value
Total no. of sections	46	37	30	41	23	177	
Total no. of nerves	1,733	1,035	934	1,480	720	5,902	
No. of nerves/section, median (IQR)	39 (23.5-50.8)	26 (16.5-39)	29 (18.5-40.3)	33 (25.5-46.5)	28 (22-37)	31 (20-43)	0.0523
No. of renal arteries/section, mean±SD	1.00±0.0	1.00±0.0	1.00±0.0	2.00±0.0	2.96±0.64		
No. of nerves/section corrected by no. of renal arteries, median (IQR)	39 (23.5-50.8)	26 (16.5-39)	29 (18.5-40.3)	16.5 (12.8-23.3)	9.3 (7.3-12)	22 (13-38)	<0.0001
The number of sections with lymph nodes, n (%)	42 (91.3)	24 (64.9)	9 (30.0)	3 (7.3)	3 (13.4)	81 (45.8)	<0.0001
Distance between LN and renal artery, mm	1.4 (1-2.8)	1.9 (1.1-3.9)	1.5 (1.1-2.6)	NA	NA	2.6 (1.8-4.7)	0.35
The number of sections with neuroganglion, n (%)	28 (60.9)	6 (16.2)	4 (13.3)	3 (7.3)	2 (8.7)	43 (24.3)	<0.0001
Distance between NG and renal artery, mm	5.4 (3.5-10.4)	7 (4.2-8.5)	1 (0.5-3.5)	NA	NA	5.2 (3.5-9.2)	0.0353
The number of sections with kidney, n (%)	0 (0)	0 (0)	0 (0)	12 (29.3)	11 (47.8)	23 (13.0)	<0.0001
Distance between kidney and renal artery, mm	0 (0-0)	0 (0-0)	0 (0-0)	NA	NA	0 (0-0)	NA
The number of sections with ureter, n (%)	0 (0)	2 (5.4)	7 (23.3)	18 (43.9)	18 (78.3)	45 (25.4)	<0.0001
Distance between ureter adrenal artery, mm	0 (0-0)	5.4 (5.1-5.7)	4.4 (3.4-5.1)	NA	NA	4.7 (3.8-5.4)	0.24
The number of sections with renal vein, n (%)	36 (78.3)	33 (89.2)	30 (100)	41 (100)	23 (100)	163 (78.3)	0.0004
Distance between renal vein and renal artery, mm	1.8 (0.9-4.8)	1.5 (1.1-3.4)	1.2 (0.9-2.1)	NA	NA	1.5 (1.0-3.1)	0.16
Total no. of nerves behind the renal vein*, n	247	181	134	128	77	767	
Percentage of the number of nerves behind the renal vein relative to the total number of nerves	14.3	17.5	14.3	8.6	10.7	13.0	

*Nerves were considered "behind" the vein when a hypothetical line extending normally between the nerve and arterial wall passed through a renal vein. IQR: interquartile range; LN: lymph nodes; NG: neuroganglion; SD: standard deviation

samples were significantly greater than in the porcine models (diameter: 4.8±0.7 mm vs 3.1±1.0 mm; p=0.0005; length: 2.8±1.0 cm vs 1.4±0.4 cm; p<0.0001; medial wall thickness: 0.45±0.10 mm vs 0.35±0.07 mm; p=0.0328) **(Supplementary Table 1)**. In both human and porcine renal arteries, the number of nerves per section corrected by the number of renal arteries in the section was greater in the proximal segments (human: 65 [50-88.8]; porcine: 39 [23.5-50.8]), decreasing moving away from the ostium (middle in human: 58 [39-83] and porcine: 26 [16.5-39]; distal in human: 47 [31.7-73] and porcine: 29 [18.5-40.3]), and lowest in the post-bifurcation sections (post-1st bifurcation in human: 22.5 [12-16] and porcine: 16.5 [12.8-23.3]; post-2nd bifurcation in human: 14.7 [8.5-18.7] and porcine: 9.3 [7.3-12]). **(Table 2, Table 3, Central illustration, Figure 1)**. Overall, the number of nerves was greater in the human arteries as compared to those from the porcine models **(Figure 1)**. Renal nerves were common in the regions between the arteries and adjacent arteries or veins, but only 3% and 13% of the renal nerves in humans and pigs, respectively, were located behind the renal vein **(Table 2, Table 3)**.

In both porcine and human samples, extra arterial structures such as lymph nodes and unspecified ganglia were randomly positioned longitudinally adjacent to the renal artery but were more common in the sections close to the ostium (median number of sections with lymph nodes in humans, proximal: 35/36 [97.2%], middle: 22/31 [71.0%], distal: 13/34 [54.2%], post-1st bifurcation: 9/49 [18.4%], and post-2nd bifurcation: 0/39 [0%]; in pigs, proximal: 42/46 [91.3%], middle: 24/37 [64.9%], distal: 9/30 [30.0%], post-1st bifurcation: 3/41 [7.3%], and post-2nd bifurcation: 3/23 [13.4%]; the median number of sections with ganglia in humans, proximal: 35/36 [97.2%], middle: 27/31 [87.1%], distal: 18/34 [75.0%], post-1st bifurcation: 13/49 [26.5%], and post-2nd bifurcation: 4/39 [10.3%]; in pigs, proximal: 28/46 [60.9%], middle: 6/37 [16.2%], distal: 4/30 [13.3%], post-1st bifurcation: 3/41 [7.3%], and post-2nd bifurcation: 2/23 [8.7%]). On the other hand, the kidney and ureter were more frequently observed surrounding the distal sections away from the ostium, especially in the post-2nd bifurcation segments (median number of sections surrounded by kidney in humans, proximal: 0/36 [0%], middle: 0/31 [0%], distal: 3/24 [12.5%], post-1st bifurcation: 12/49 [24.5%], and post-2nd bifurcation: 23/39 [59.0%]; in pigs, proximal: 0/46 [0%], middle: 2/37 [5.4%], distal: 7/30 [23.3%], post-1st bifurcation: 18/41 [43.9%], and post-2nd bifurcation: 18/23 [78.3%]; the median number of sections surrounded by ureter in humans, proximal: 0/36 [0%], middle: 0/31 [0%], distal: 1/34 [4.2%], post-1st bifurcation: 8/49 [16.3%], and post-2nd bifurcation: 14/39 [35.9%]; in pigs, proximal: 0/46 [0%], middle: 2/37 [5.4%], distal: 7/30 [23.3%], post-1st bifurcation: 18/41 [43.9%], and post-2nd bifurcation: 18/23 [78.3%]). The renal vein was more frequently observed in distal sections moving away from the ostium and was seen in most sections after bifurcation **(Table 2, Table 3, Figure 2)**. When comparing the prevalence of perirenal artery structures, neuroganglia were more frequently observed in humans than in pigs **(Figure 2)**.

In terms of the distance from peri-arterial structures to the renal artery, the distances from lymph nodes and renal veins were greater in humans than in the porcine subjects. In contrast, the distance

CENTRAL **ILLUSTRATION** **Representative images of untreated human and treated porcine renal arteries and their surrounding tissues in various locations.**

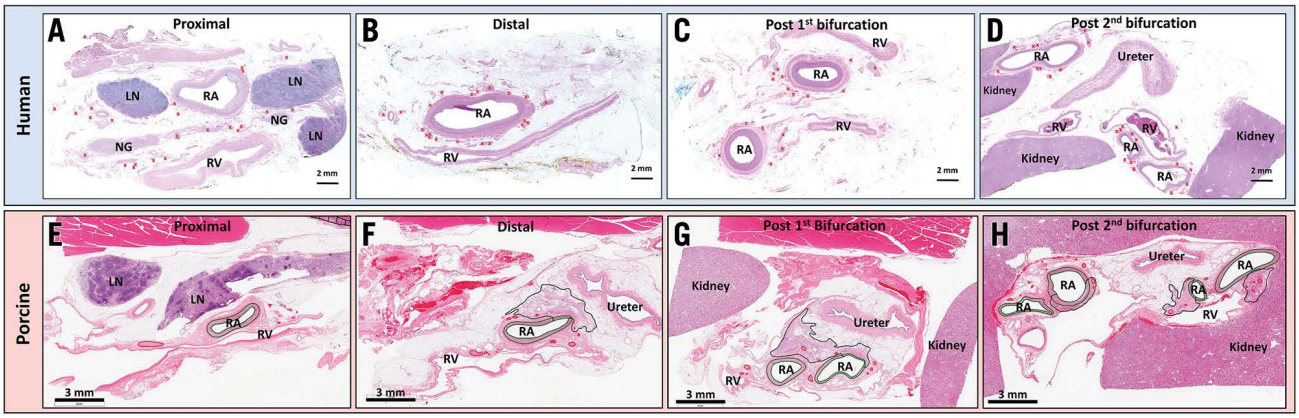

Human (A) and porcine (E) proximal renal artery segments. Peri-arterial structures, such as lymph nodes (LN) and neuroganglia (NG), are frequently observed around the renal artery (RA). Peri-arterial nerves are seen near and far from the renal arteries (red crosses in human and red circles in porcine sections) but are not found "behind" the renal vein (RV). In the porcine RA section, the areas where treatment changes are seen are surrounded by a black line. Human (B) and porcine (F) distal renal artery segments. Peri-arterial structures (i.e., LN and NG) are not seen. Peri-arterial nerves are located closer to the renal artery than the proximal segments, and not seen "behind" the RV. Human (C) and porcine (G) post-1st bifurcation segments. Two branched renal arteries are observed. In the porcine section, the ureter and kidney are visible. Human (D) and porcine (H) post-2nd bifurcation segments. The kidney and ureter are seen in the histologic sections. Peri-arterial nerves are located close to the renal arteries. All sections are stained with haematoxylin and eosin.

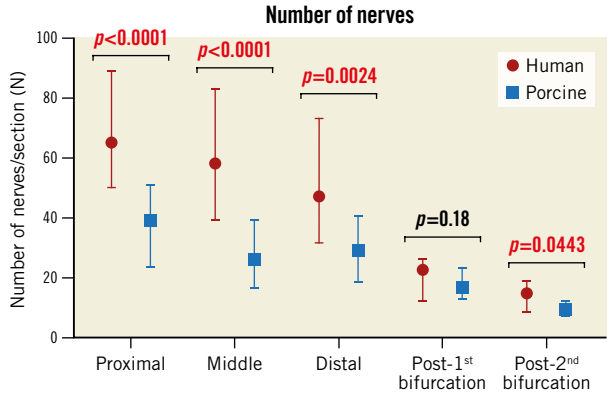

Figure 1. *The number of peri-arterial nerves in human and porcine renal arteries in proximal, middle, distal, post-1st bifurcation, and post-2nd bifurcation segments. The numbers were corrected for the number of renal arteries seen in sections. Values are shown as median and interquartile ranges.*

from neuroganglia to the renal artery was greater in pigs as compared to humans **(Table 2, Table 3, Supplementary Figure 1)**. No differences were observed in these distances for either the ureter or kidney **(Table 2, Table 3, Supplementary Figure 1)**.

RADIOFREQUENCY ABLATION PATTERNS: PORCINE MODEL

A total of 375 histologic sections from 12 pigs from the 7-day group and 580 sections from 16 pigs from the 28-day group were included in the semiquantitative analysis. RF lesions in porcine renal arteries were characterised by hyalinised media at the point of electrode contact. Outside the vessel wall, RF lesions primarily consisted of necrosis and inflammation of perivascular adipose tissue following RF ablation **(Central illustration)**. Substantial neointima formation was not observed in any treated arteries (N=56). The scores for RF-induced changes were observed rarely and, if seen, were minimal in perivascular lymph nodes (0.03±0.06 at 7 days and 0.01±0.03 at 28 days), in subjacent skeletal muscle (0.09±0.09 at 7 days and 0.02±0.04 at 28 days), in the ureter (0.03±0.05 at 7 days and 0±0 at 28 days), and in the kidneys (0.18±0.14 at 7 days and 0.03±0.06 at 28 days). No RF damage was observed in surrounding adrenal glands at either 7 or 28 days. Scores for all peri-arterial tissues were nominally lower in the 28-day post-RDN group as compared to the 7-day cohort. The score for nerve necrosis was 0.98±0.23 at 7 days and significantly decreased at 28 days (0.75±0.20; p=0.01), suggesting a healing process. On the other hand, there was no significant difference in downstream axonal loss (i.e., nerve body atrophy) between 7 days and 28 days (1.4±0.48 vs 1.63±0.41; p=0.20) **(Figure 3)**.

Discussion

Nerve destruction resulting from percutaneous catheter-based renal denervation is determined by the interaction of multiple factors, including the energy source, delivery mechanism, and the local anatomic and haemodynamic physical environment. The main finding of our analysis is that the distribution of nerve

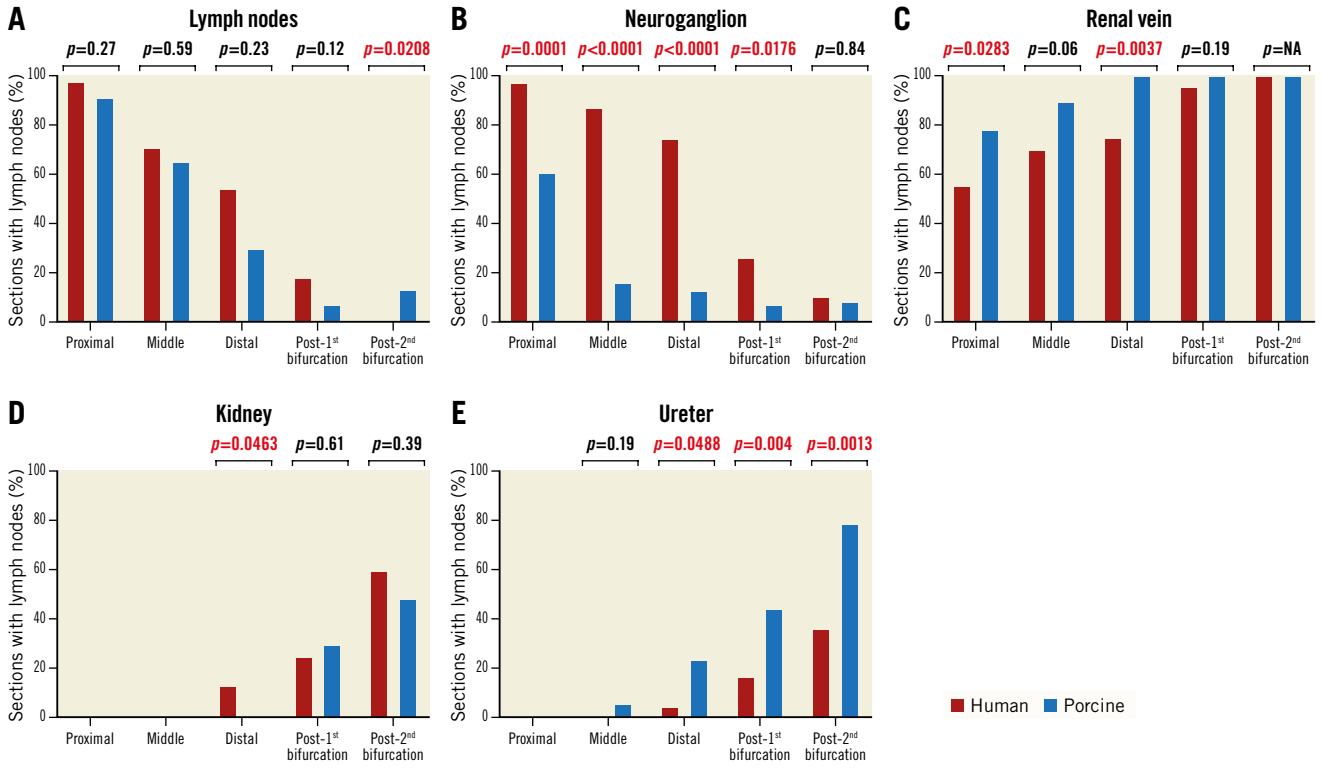

Figure 2. *Prevalence of organs surrounding human and porcine renal arteries in proximal, middle, distal, post-1st bifurcation, and post-2nd bifurcation segments. The presence of surrounding non-target organs was relatively minimal in the post-1st bifurcation sections for both the human and porcine samples. Number of sections analysed at each location in human: proximal 36, middle 31, distal 24, post-1st bifurcation 43, and post-2nd bifurcation 45; in porcine: proximal 46, middle 37, distal 30, post-1st bifurcation 41, and post-2nd bifurcation 23.*

tissues and the relative distribution of extravascular anatomic structures along the renal artery between the aorta and kidney was similar between humans and commonly studied domestic pigs. We performed RF ablation in porcine renal arteries, but not in humans, and demonstrated successful peri-arterial nerve treatment with minimal perivascular tissue damage. Since the

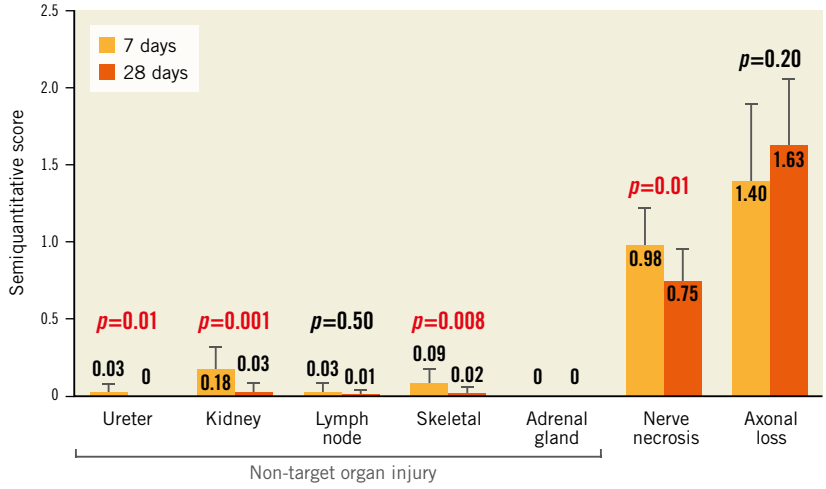

Figure 3. *Mean semiquantitative scoring of histological tissue samples from porcine model. Despite nerve necrosis at the site of RF ablation and downstream axonal loss (nerve atrophy), minimal cell disruption was observed to adjacent tissues including the ureter, kidney, lymph, skeletal muscle, and adrenal glands at 7 days following RF ablation. Non-target organ scores decreased even further at 28 days. However, substantial axonal loss persisted at 28 days. Scoring: 0=no changes; 1=minimal changes; 2=notable changes not effacing pre-existing tissue elements or limited to a small tissue area; 3=overwhelming feature involving large tissue areas. Values are shown as mean with error bar (standard deviation). P-values determined via unpaired t-test.*

anatomies are comparable, especially in terms of the presence of extravascular structures, RF ablation to human renal arteries would result in minimal damage to these structures. These observed anatomic similarities validate the translational value of the normotensive porcine model to evaluate the effects of percutaneous RDN on microscopic tissue. Histological analysis may thus reliably identify critical factors to maximise the probability of both a safe and effective human procedure, thereby further improving patient outcomes.

Renal sympathetic nerves originate from multiple sources including the celiac and aortico-renal ganglia, thoracic and lumbar splanchnic nerves and the mesenteric nerves and superior mesenteric ganglion. Post-ganglionic fibres enter the kidney through the renal plexus which may not be fully formed in the proximal renal artery[11]. The present results confirm and extend previous anatomic reports[11,12] indicating that sympathetic nerve ganglia are randomly distributed in the vicinity of the renal artery and their precise location is not consistent between individuals. The implications of ablating non-renal ganglia via RF-RDN or other methods are uncertain. However, focusing ablation on the distal portion of the main artery and the proximal branch vessels seems prudent, since the non-specific ganglia are less likely to be affected by lesions in these areas. Furthermore, the presently observed lack of significant or sustained collateral tissue damage **(Figure 3)** suggests that distal RF ablation beyond the main bifurcation would not result in collateral tissue damage relative to main renal artery treatment.

RENAL ARTERY SAFETY

INFLUENCE OF SURROUNDING ANATOMIC STRUCTURES AND COMPOSITION

The distribution of peri-arterial nerves in both human and porcine renal arteries in the current study is consistent with previous human autopsy studies[7,13] showing that some nerves observed proximally most likely diverge to other retroperitoneal or mesenteric organs in both human and porcine samples. However, these prior studies did not encompass the relationship between peri-arterial nerves and surrounding anatomic structures, such as lymph nodes, neuroganglia, and renal veins. Also, we previously performed and reported safety assessments using the legacy Symplicity Catheter in porcine renal arteries[9]. However, the current study adds comprehensive safety information for the newer-generation multielectrode Symplicity Spyral catheter, which is being clinically used in countries where this technology is approved by the governing bodies. Unlike the clear anatomic divisions between the endothelium, media, and adventitia, the boundaries between the adventitia and the extravascular space are difficult to discern. The relatively low conductivity of adipose tissue compared to other tissues and fluids results in greater resistive loss and fat tissue therefore heats preferentially. This phenomenon facilitates nerve destruction during RF ablation, since the renal nerves tend to be embedded within the adventitial adipose tissue[14,15]. Likewise, adjacent lymph nodes, veins, and other arteries tend not to be damaged by temperature as higher electrical conductivity and convective heat conduction from flowing fluid deter the achievement of higher temperatures in these tissues. Moreover, in the primary branches, the kidneys and ureters were less frequently observed than in the secondary branches, suggesting that the ablation to the primary branches is less likely to affect these organs.

DIFFERENTIAL NERVE LOCATION

A previous study showed that the relative positioning of RF electrodes in the renal arteries adjacent to a vein may be disadvantageous because venous blood dissipates heat, reduces the depth of excision, and shields surrounding nerves from the intended treatment[15,16]. Intentional positioning of any current RDN therapy within the artery relative to extravascular structures is not achievable with current fluoroscopically-guided procedural techniques. However, less than 3% of human renal nerves were observed "behind" an adjacent vein and were almost always confined to the adventitia and extravascular space between the artery and the vein. Renal nerve paths tended to anatomically track the artery but not the veins, perhaps due to their known function in innervating effector arterioles (which are absent in veins)[17]. The lack of anatomical association of renal nerves with the veins suggests minimal potential thermal protection of renal nerves from RF ablation.

Renal denervation beyond the main bifurcation has been previously demonstrated to result in larger changes in renal cortical norepinephrine content with lower variability between subjects[8]. The kidneys and ureter were not commonly observed until beyond the second level branches and denervation in the primary branches did not impact the kidneys and ureter **(Figure 2)**. These observations are in line with recent clinical analyses of RDN with RF energy, providing evidence for the safety of RDN with respect to renal function[18,19,20].

Limitations

The present study has the following limitations. First, human tissue studies were collected from cadavers for anatomic studies only, not obtained from RDN-treated patients. As such, the human cadaver data only represent untreated samples of human renal anatomy. Secondly, the anatomy of porcine arteries may vary somewhat from humans. Specifically, the vessels in young pigs generally have thinner walls, smaller renal arteries, and no atherosclerotic disease in comparison to elderly human patients. However, the average magnitude difference in medial wall thickness was about 0.1 mm, and thus the porcine model results for lesion formation are likely still appropriate. Young pigs also appear to have a smaller volume of perirenal and peri-arterial adipose tissue as compared to humans. We did however observe distinct similarities in the anatomic distribution of the perivascular structures between human and porcine samples, which validates the appropriateness of the pig model to investigate the safety of RDN.

Conclusions

In conclusion, we observed similar relative distribution of nerve tissues and extravascular anatomic structures along the renal artery between the aorta and kidney between human and pig tissue, supporting the translatability of histological analyses of RF-RDN in the porcine model. Human renal nerves are infrequently located behind veins and thus not thermally "protected" from RF heating. Distal ablation beyond the first bifurcation was not associated with additional damage to the kidneys or ureter in the porcine model compared to main artery ablation.

Impact on daily practice

Preclinical models have played an important role in radiofrequency renal denervation, which are unobtainable from human studies. The distribution of nerve tissues and the relative distribution of extravascular anatomic structures along the renal artery was similar between humans and pigs. This study validated the translational value of the normotensive porcine model for renal denervation, which has an impact on further improvement of renal denervation technologies.

Acknowledgements

The authors would like to thank the teams at the CVPath Institute, Inc. and Medtronic.

Funding

The animal study in the current study was funded by Medtronic, while the cadaver study in the current study was partially supported by CVPath Institute Inc. a not-for-profit 501©(3) research Institute.

Conflict of interest statement

A. Sharp receives consulting fees/honoraria from Medtronic, Philips and ReCor Medical. F. Mahfoud is supported by Deutsche Gesellschaft für Kardiologie and Deutsche Forschungsgemeinschaft (SFB 219); and has received scientific support and/or speaker honoraria from Bayer, Boehringer Ingelheim, Medtronic, Merck, and ReCor Medical. S. Tunev is a full-time employee of Medtronic. J. Trudel is a full-time employee of Medtronic. D.A. Hettrick is a full-time employee of Medtronic. M. Schlaich is supported by an NHMRC Senior Research Fellowship; and has received consulting fees and/or travel and research support from Medtronic, Abbott, Novartis, Servier, Pfizer, and Boehringer Ingelheim. D. Lee reports grants from and serves on the advisory board for Medtronic; and research support from Ablative Solutions. D.E. Kandzari reports institutional research/grant support from Medtronic CardioVascular and Ablative Solutions and personal consulting honoraria from Medtronic CardioVascular and Ablative Solutions. A.V. Finn reports consulting honoraria from Amgen, Abbott Vascular, Biosensors, Boston Scientific, CeloNova, Cook Medical, CSI, Lutonix Bard, Medtronic, and Terumo. R. Virmani reports institutional grant/research support from NIH-HL141425, Leducq Foundation Grant, 4C Medical, 4Tech, Abbott Vascular, Ablative Solutions, Absorption Systems, Advanced NanoTherapies, AerWave Medical, Alivas, Amgen, Asahi Medical, Aurios Medical, Avantec Vascular, BD, Biosensors, Biotronik, Biotyx Medical, Bolt Medical, Boston Scientific, Canon USA, Cardiac Implants, Cardiawave, CardioMech, Cardionomic, CeloNova, Cerus EndoVascular, Chansu Vascular Technologies, Childrens National Medical Center, Concept Medical, Cook Medical, Cooper Health, Cormaze Technologies GmbH, CRL/AccelLab, Croivalve, CSI, Dexcom, Edwards Lifesciences, Elucid Bioimaging, eLum Technologies, Emboline, Endotronix, Envision, Filterlex, Imperative Care, Innovalve, Innovative Cardiovascular Solutions, Intact Vascular, Interface Biologics, InterShunt Technologies, InVatin Technologies, Lahav CRO, LimFlow, L&J Biosciences, Lutonix, Lyra Therapeutics, Mayo Clinic, Maywell, MD Start, MedAlliance, Medanex, Medtronic, Mercator, Microport, Microvention, Neovasc, Nephronyx, Nova Vascular, Nyra Medical, Occultech, Olympus, Ohio Health, OrbusNeich, Ossio, Phenox, Pi-Cardia, Polares Medical, Polyvascular, PulseTherapeutics, Profusa, ProKidney, Protembis, Pulse Biosciences, Qool Therapeutics, Recombinetics, ReCor Medical, Regencor, Renata Medical, Restore Medical, Ripple Therapeutics, Rush University, Sanofi, Shockwave, Sahajanand Medical Technologies, SoundPipe, Spartan Micro, SpectraWAVE, Surmodics, Terumo, the Jacobs Institute, Transmural Systems, Transverse Medical, TruLeaf Medical, UCSF, UPMC, Vascudyne, Vesper, Vetex Medical, Whiteswell, W.L. Gore, and Xeltis; has received consulting honoraria from Abbott Vascular, Boston Scientific, CeloNova, OrbusNeich, Terumo, W.L. Gore, Edwards Lifesciences, Cook Medical, CSI, ReCor Medical, SinoMedical Sciences Technology, Surmodics, and Bard BD; and is a scientific advisory board member of Medtronic and Xeltis. The other authors have no conflicts of interest to declare.

References

1. Mills KT, Stefanescu A, He J. The global epidemiology of hypertension. *Nat Rev Nephrol*. 2020;16:223-37.

2. NCD Risk Factor Collaboration (NCD-RisC). Worldwide trends in hypertension prevalence and progress in treatment and control from 1990 to 2019: a pooled analysis of 1201 population-representative studies with 104 million participants. *Lancet.* 2021;398:957-80.

3. Kandzari DE, Böhm M, Mahfoud F, Townsend RR, Weber MA, Pocock S, Tsioufis K, Tousoulis D, Choi JW, East C, Brar S, Cohen SA, Fahy M, Pilcher G, Kario K; SPYRAL HTN-ON MED Trial Investigators. Effect of renal denervation on blood pressure in the presence of antihypertensive drugs: 6-month efficacy and safety results from the SPYRAL HTN-ON MED proof-of-concept randomised trial. *Lancet.* 2018;391:2346-55.

4. Böhm M, Kario K, Kandzari DE, Mahfoud F, Weber MA, Schmieder RE, Tsioufis K, Pocock S, Konstantinidis D, Choi JW, East C, Lee DP, Ma A, Ewen S, Cohen DL, Wilensky R, Devireddy CM, Lea J, Schmid A, Weil J, Agdirlioglu T, Reedus D, Jefferson BK, Reyes D, D'Souza R, Sharp ASP, Sharif F, Fahy M, DeBruin V, Cohen SA, Brar S, Townsend RR; SPYRAL HTN-OFF MED Pivotal Investigators. Efficacy of catheter-based renal denervation in the absence of antihypertensive medications (SPYRAL HTN-OFF MED Pivotal): a multicentre, randomised, sham-controlled trial. *Lancet.* 2020;395:1444-51.

5. Azizi M, Schmieder RE, Mahfoud F, Weber MA, Daemen J, Davies J, Basile J, Kirtane AJ, Wang Y, Lobo MD, Saxena M, Feyz L, Rader F, Lurz P, Sayer J, Sapoval M, Levy T, Sanghvi K, Abraham J, Sharp ASP, Fisher NDL, Bloch MJ, Reeve-Stoffer H, Coleman L, Mullin C, Mauri L; RADIANCE-HTN Investigators. Endovascular ultrasound renal denervation to treat hypertension (RADIANCE-HTN SOLO): a multicentre, international, single-blind, randomised, sham-controlled trial. *Lancet.* 2018;391:2335-45.

6. Azizi M, Sanghvi K, Saxena M, Gosse P, Reilly JP, Levy T, Rump LC, Persu A, Basile J, Bloch MJ, Daemen J, Lobo MD, Mahfoud F, Schmieder RE, Sharp ASP, Weber MA, Sapoval M, Fong P, Pathak A, Lantelme P, Hsi D, Bangalore S, Witkowski A, Weil J, Kably B, Barman NC, Reeve-Stoffer H, Coleman L, McClure CK, Kirtane AJ; RADIANCE-HTN investigators. Ultrasound renal denervation for hypertension resistant to a triple medication pill (RADIANCE-HTN TRIO): a randomised, multicentre, single-blind, sham-controlled trial. *Lancet.* 2021;397:2476-86.

7. Sakakura K, Ladich E, Cheng Q, Otsuka F, Yahagi K, Fowler DR, Kolodgie FD, Virmani R, Joner M. Anatomic assessment of sympathetic peri-arterial renal nerves in man. *J Am Coll Cardiol.* 2014;64:635-43.

8. Mahfoud F, Tunev S, Ewen S, Cremers B, Ruwart J, Schulz-Jander D, Linz D, Davies J, Kandzari DE, Whitbourn R, Böhm M, Melder RJ. Impact of Lesion Placement on Efficacy and Safety of Catheter-Based Radiofrequency Renal Denervation. *J Am Coll Cardiol.* 2015;66:1766-75.

9. Sakakura K, Tunev S, Yahagi K, O'Brien AJ, Ladich E, Kolodgie FD, Melder RJ, Joner M, Virmani R. Comparison of histopathologic analysis following renal sympathetic denervation over multiple time points. *Circ Cardiovasc Interv.* 2015;8:e001813-.

10. Sakakura K, Ladich E, Edelman ER, Markham P, Stanley JR, Keating J, Kolodgie FD, Virmani R, Joner M. Methodological standardization for the pre-clinical evaluation of renal sympathetic denervation. *JACC Cardiovasc Interv.* 2014;7:1184-93.

11. García-Touchard A, Maranillo E, Mompeo B, Sanudo JR. Microdissection of the Human Renal Nervous System: Implications for Performing Renal Denervation Procedures. *Hypertension.* 2020;76:1240-6.

12. Mompeo B, Maranillo E, Garcia-Touchard A, Larkin T, Sanudo J. The gross anatomy of the renal sympathetic nerves revisited. *Clin Anat.* 2016;29:660-4.

13. Sato Y, Kawakami R, Jinnouchi H, Sakamoto A, Cornelissen A, Mori M, Kawai K, Guo L, Coleman L, Nash S, Claude L, Barman NC, Romero M, Kolodgie FD, Virmani R, Finn AV. Comprehensive Assessment of Human Accessory Renal Artery Periarterial Renal Sympathetic Nerve Distribution. *JACC Cardiovasc Interv.* 2021;14:304-15.

14. Coates P, Tunev S, Trudel J, Hettrick DA. Time, Temperature, Power, and Impedance Considerations for Radiofrequency Catheter Renal Denervation. *Cardiovasc Revasc Med.* 2022;42:171-7.

15. Tzafriri AR, Keating JH, Markham PM, Spognardi AM, Stanley JR, Wong G, Zani BG, Highsmith D, O'Fallon P, Fuimaono K, Mahfoud F, Edelman ER. Arterial microanatomy determines the success of energy-based renal denervation in controlling hypertension. *Sci Transl Med.* 2015;7:285ra65.

16. Tzafriri AR, Mahfoud F, Keating JH, Spognardi AM, Markham PM, Wong G, Highsmith D, O'Fallon P, Fuimaono K, Edelman ER. Procedural and Anatomical Determinants of Multielectrode Renal Denervation Efficacy. *Hypertension.* 2019;74:546-54.

17. Mitchell GA. The nerve supply of the kidneys. Acta Anat (Basel). 1950;10:1-37.

18. Mahfoud F, Böhm M, Schmieder R, Narkiewicz K, Ewen S, Ruilope L, Schlaich M, Williams B, Fahy M, Mancia G. Effects of renal denervation on kidney function and long-term outcomes: 3-year follow-up from the Global SYMPLICITY Registry. *Eur Heart J.* 2019;40:3474-82.

19. Ott C, Mahfoud F, Schmid A, Toennes SW, Ewen S, Ditting T, Veelken R, Ukena C, Uder M, Böhm M, Schmieder RE. Renal denervation preserves renal function in patients with chronic kidney disease and resistant hypertension. *J Hypertens.* 2015;33:1261-6.

20. Ott C, Mahfoud F, Mancia G, Narkiewicz K, Ruilope LM, Fahy M, Schlaich MP, Böhm M, Schmieder RE. Renal denervation in patients with versus without chronic kidney disease: results from the global SYMPLICITY Registry with follow-up data of 3 years. *Nephrol Dial Transplant.* 2022;37:304-10.

Supplementary data

Supplementary Table 1. Histomorphometric analysis of the main renal arteries in humans and pigs.

Supplementary Figure 1. Comparison of the distance from the renal artery to the peri-arterial surrounding structures.

The supplementary data are published online at: https://eurointervention.pcronline.com/doi/10.4244/EIJ-D-22-00369

Supplementary data

Supplementary Table 1. Histomorphometric analysis of the main renal arteries in humans and pigs.

	Human	Porcine	p-value
No. of renal arteries, n	20	16	-
Main renal arterial length from ostium to 1st bifurcation, cm	2.8 ± 1.0	1.4 ± 0.4	<0.0001
Main renal arterial diameter in histology, mm	4.8 ± 0.7	3.1 ± 1.0	0.0005
Main renal artery medial wall thickness, mm	0.45 ± 0.10	0.35 ± 0.07	0.0328

Values are shown as mean ± standard deviation.

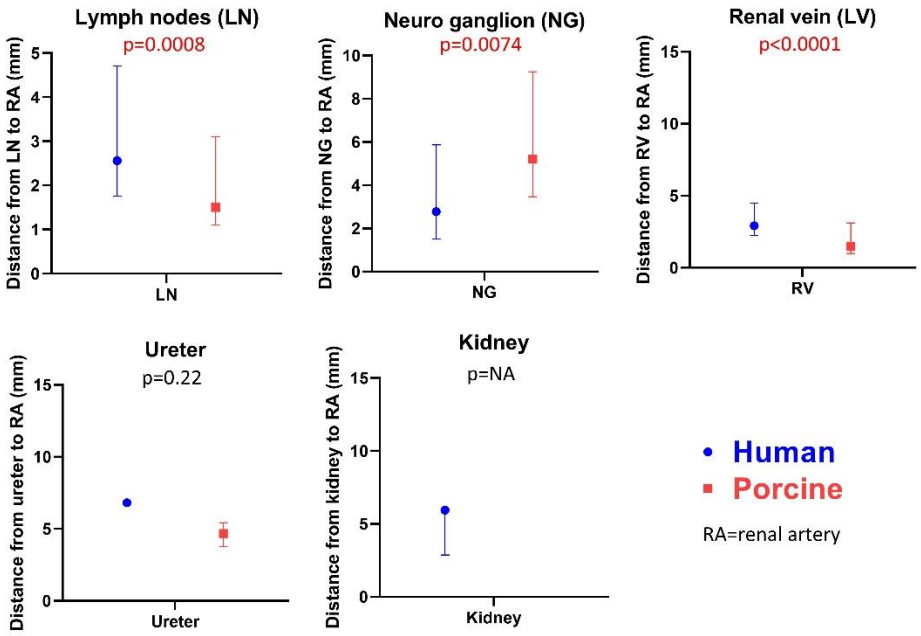

Supplementary Figure 1. Comparison of the distance from the renal artery to the peri-arterial surrounding structures.

Post-bifurcation sections were excluded from this analysis.